AIP Journal of Applied Physics

Strain and electric field induced electronic properties of two-dimensional hybrid bilayers of transition-metal dichalcogenides

Munish Sharma, Ashok Kumar, P. K. Ahluwalia, and Ravindra Pandey

Citation: Journal of Applied Physics **116**, 063711 (2014); doi: 10.1063/1.4892798
View online: http://dx.doi.org/10.1063/1.4892798
View Table of Contents: http://scitation.aip.org/content/aip/journal/jap/116/6?ver=pdfcov
Published by the AIP Publishing

Strain and electric field induced electronic properties of two-dimensional hybrid bilayers of transition-metal dichalcogenides

Munish Sharma,[1,a)] Ashok Kumar,[1] P. K. Ahluwalia,[1,a)] and Ravindra Pandey[2]
[1]*Department of Physics, Himachal Pradesh University, Shimla 171005, India*
[2]*Department of Physics, Michigan Technological University, Houghton, Michigan 49931, USA*

(Received 19 May 2014; accepted 29 July 2014; published online 14 August 2014)

Tunability of the electronic properties of two-dimensional bilayer hetero structures of transition-metal dichalcogenides (i.e., MX_2-$M'X'_2$ with (M, M′ = Mo, W; X, X′ = S, Se) is investigated. Application of both strain and electric field is found to modify the band gap and carrier effective mass in the hybrid bilayers considered. The calculated results based on density functional theory suggest that the tensile strain considerably changes the band gap of semiconducting bilayers; it makes the band gap to be indirect, and later initiates the semiconductor-to-metal transition. Application of the external electric fields, on the other hand, shows asymmetric variation in the band gap leading to the closure of the gap at about 0.5–1.0 V/Å. Tuning of the band gap and carrier effective mass in such a controlled manner makes the hybrid bilayers of transition metal dichalcogenides to be promising candidates for application in electronic devices at nanoscale. © *2014 AIP Publishing LLC*. [http://dx.doi.org/10.1063/1.4892798]

I. INTRODUCTION

Two dimensional (2D) layered transition metal dichalcogenides (TMDs) have attracted a great deal of interest[1–9] due to their distinctive novel physical and chemical properties, since the isolation of MoS_2[10,11] by the mechanical exfoliation technique similar to one applied to graphene. The layered TMDs are the class of materials with formula MX_2 (where M is metal atom X is the chalcogen atom) having the hexagonal structure with space group $P6_3/mmc$.[12] It is noteworthy that monolayers of TMDs are not one atom thick as graphene, but are tri-atomic thick layers consisting of metal atoms sandwiched between two layers of chalcogen atoms. In plane atoms are bonded via strong covalent bonds, while the adjacent layers along the thickness direction are bonded together by a weak van der Wall forces which are strong enough to hold them together. Therefore, the TMDs layered materials offer interesting possibilities to design and fabricate electronic devices involving hetero structures. Recently, the possibility of making such hetero structure multi-layer systems has been reported in the scientific literature.[13,14] For example, the direct band gap of TMD monolayers is tunable with the application of the mechanical strain.[5,15–17] On the other hand, theoretical investigations suggest that the direct band gap at high symmetric "K" point (in a TMD monolayer) can be preserved in multi-layers by carefully designing hetero structures.[18–20] The experimental possibility to synthesize hetero structures[14,21] and theoretical predictions to control the direct band gap character via composition control have motivated us to investigate the possibility of tailoring of band gap of the TMD hetero structures by the external factors which have not been explored much so far. We examine the effect of both intrinsic and extrinsic strains, e.g., bi-axial tensile (+a+b), in-plane bi-axial compression (−a−b), out-of-plane compression (−c) strain together with the perpendicular electric field on the electronic properties, including electronic band gap, deformation potentials (DPs), and carrier effective masses of hetero bilayers of TMDs.

II. COMPUTATIONAL DETAILS

First principle calculations were performed by means of density functional theory (DFT) as implemented in the pseudo-potential and numerical atomic orbitals (NAOs) basis sets based SIESTA code.[22] In order to account for electron-ion interactions, we used the well tested Troullier Martin, norm conserving, relativistic pseudo-potential[23] in a fully separable Kleinman and Bylander form. The exchange and correlation energies were treated within the generalized gradient approximation (GGA) according to Perdew-Burke-Ernzerhof (PBE) parameterization. The double zeta polarized (DZP) numerical atomic orbital basis set with the confinement energy 30 meV was used to expand the Kohn-Sham orbitals.

The structures were relaxed until the force on each atom was less than 0.04 eV/Å. The 200 Ry mesh cutoff was used for reciprocal space expansion of the total charge density. The Brillouin zone was sampled using Monkhorst-Pack $15 \times 15 \times 3$ of k-points. In the supercell, the interaction between the two adjacent bilayers was eliminated by introducing a sufficient vacuum of ∼25 Å along the *z*-direction, i.e., perpendicular to surface.

The calculated structural parameters, namely, lattice constant, intraplanar bond length (R), and interplanar separation, Z are given in Table I. The calculated lattice parameters are found to be in good agreement with the previously reported values obtained using density functional theory (Table I).[19,20,24–26] For example, the interlayer separation and the lattice constant for the MoS_2-MoS_2 bilayer are found to be 4.17 and 3.22 Å, respectively, which are in very good agreement with the previously reported values[20,24] of 4.14

a)Authors to whom correspondence should be addressed. Electronic addresses: munishsharmahpu@live.com and pk_ahluwalia7@yahoo.com

TABLE I. Lattice constants, interplanar separation (Z), intraplanar bond length (R), and binding energy (E_B) for the AB-stacked bilayers. For comparison reported values have been shown wherever available.

Bilayer type	Material MX_2-$M'X'_2$	Lattice constant	Z (Å)	R (Å)	
				M-X	M′-X′
I	MoS_2-MoS_2	3.22, 3.2[a]	4.17, 4.14[b]	2.44, 2.43[c]	…
	$MoSe_2$-$MoSe_2$	3.36	3.50, 3.88[b]	2.57	…
	WS_2-WS_2	3.23	4.17, 4.31[b]	2.46	…
	WSe_2-WSe_2	3.37	3.45	2.58	…
II	MoS_2-$MoSe_2$	3.28, 3.32[d], 3.25[e]	4.13	2.46, 2.43[e]	2.55, 2.53[e]
	WS_2-WSe_2	3.30, 3.25[e]	3.42	2.47, 2.439[e]	2.57, 2.54[e]
III	MoS_2-WS_2	3.22, 3.18[d]	4.15	2.44	2.45
	$MoSe_2$-WSe_2	3.36	3.69	2.57	2.58
IV	MoS_2-WSe_2	3.29, 3.24[f]	4.11	2.46	2.57
	$MoSe_2$-WS_2	3.29	3.54	2.55	2.47

[a]Reference 20.
[b]Reference 24.
[c]Reference 15.
[d]Reference 19.
[e]Reference 25.
[f]Reference 26.

and 3.2 Å, respectively. Similarly, in the MoS_2-$MoSe_2$ hetero bilayer, our calculated lattice constant of 3.28 Å is found to be in very close agreement with the recently reported value of 3.32 Å.[19] These findings affirm the accuracy and reliability of our modelling elements used in calculations. Furthermore, our group has done extensive work on 2D materials, including graphene, BN, and GaN monolayers using the approaches which use either atomic orbitals (e.g., SIESTA) or plane waves (e.g., VASP) as basis sets for electronic structure calculations. The results of these approaches are in excellent agreement with each other in terms of predicting stability, structural, and electronic properties of 2D materials.[27,28]

The equilibrium configuration of the hetero bilayer was used to calculate the electronic structure of un-strained/zero electric field hetero structures. The applied mechanical strain is defines as $e = \Delta a/a_0$, where a_0 is equilibrium lattice constant and Δa is change in the lattice constant simulating the strain. The two types of in-plain strains, namely, bi-axial tensile (i.e., expansion) strain (+a+b) and compression (−a−b) strain was applied along x and y-axis. The out-of-plane (vertical) compression strain (−c) was simulated by decreasing the interlayer distance of hetero bilayers.

III. RESULTS AND DISCUSSIONS

Following the stacking convention used for hetero bilayers, the AB-stacked TMDs bilayer consists of the case in which the metal atoms of the second layer are directly above the chalcogen atoms of the first layer and vice versa. On the other hand, the AA-stacked, bilayer has the metal atoms of the first and second layer directly above each other.[6] Note that AB-stacked TMDs bilayers are predicted to be the most stable bilayer configuration for TMDs.[6,24,29] Our calculated value of binding energy (E_B) of all the considered hetero structures is very small of the order of 0.03 eV which indicates the presence of the weak van der Waals interactions in these layered materials. E_B is defined as total energy of a bilayer minus the sum of total energies of corresponding constituent monolayers. In the following, we consider four types of MX_2-$M'X'_2$ bilayers (see Figure 1) for electronic structure calculations:

- Type-I, MX_2-MX_2 (i.e., MoS_2-MoS_2, $MoSe_2$-$MoSe_2$, WS_2-WS_2, and WSe_2-WSe_2), bilayers consist of the stacking of two monolayers of TMDs with same metal and chalcogen atoms.
- Type-II, MX_2-MX'_2 (i.e., MoS_2-$MoSe_2$ and WS_2-WSe_2), bilayers have different chalcogen atoms on the constituent monolayers.

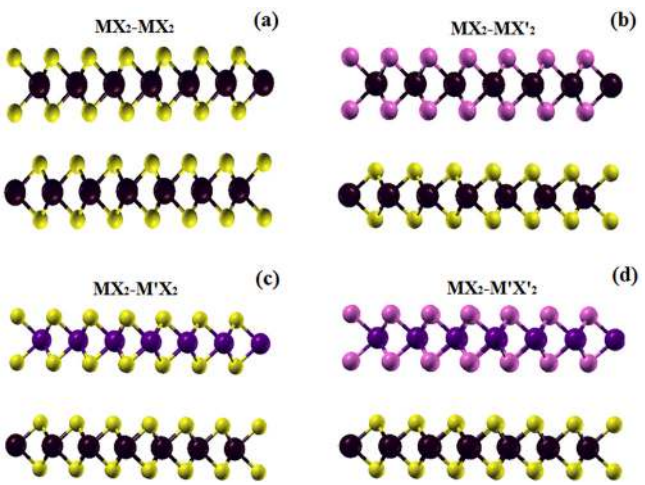

FIG. 1. Ball and stick models representing the AB-stacked bilayer heterostructures of TMDs. (a) Type-I, MX_2-MX_2 (i.e., MoS_2-MoS_2, $MoSe_2$-$MoSe_2$, WS_2-WS_2, and WSe_2-WSe_2) bilayer, (b) Type-II, MX_2-MX'_2 (i.e., MoS_2-$MoSe_2$ and WS_2-WSe_2) bilayer, (c) Type-III, MX_2-$M'X_2$, (i.e., MoS_2-WS_2 and $MoSe_2$-WSe_2) bilayer, and (d) Type-IV, MX_2-$M'X'_2$ (i.e., MoS_2-WSe_2, $MoSe_2$-WS_2) bilayer.

- Type-III, MX_2-$M'X_2$, (i.e., MoS_2-WS_2 and $MoSe_2$-WSe_2), bilayers consist of different transition metal atoms on constituent monolayers.
- Type-IV, MX_2-$M'X'_2$ (i.e., MoS_2-WSe_2, $MoSe_2$-WS_2), bilayers have both different chalcogen and metal atoms on the constituent monolayers.

A. Effect of induced intrinsic strain on the electronic properties

In the bilayer configuration, the lattice mismatch between the two constituent units of a hetero bilayer system leads to strain intrinsically within the system itself. Such a strain in the system is termed as intrinsic strain. For TMDs, the lattice constants of hetero bilayers (Type-II, Type-III and Type-IV) lie between those of bilayers of the constituting units (Table I). Therefore, one unit of hetero bilayer will undergo tensile strain with $\varepsilon_1 = x(a_y/a_x - 1)$ and the other unit will undergo compression strain $\varepsilon_2 = x(a_x/a_y - 1)$, where $x = 1/2$ and a_x, a_y are lattice constants of constituting bilayers.

1. Band structure

The induced intrinsic strain due to lattice mismatch at the interface of two hetero layers introduces significant impact on the electronic band gap in hetero bilayers. The induced tensile/compression strain and the calculated band gap of various bilayers are listed in Table II. Note that homo bilayers posses indirect band gap, while all the hetero bilayers, except MoS_2-WS_2, are direct band gap materials. However, the difference between indirect and direct band gap for MoS_2-WS_2 was found to be very small of the order of 20 meV. The band gap reduction in the hetero structures as compared with homo structures might be due to phenomenon of band gap offset, i.e., charge carriers are confined to different layers.[30]

2. Deformation potential

Next, we investigate the effect of induced strain on the band gap deformation potential, which is a useful parameter for device modeling.[31–33]

Since the induced intrinsic strain is small of the order of 2%, the deformation potential for induced tensile and compression strain can be defined as $(E_{x-y} - E_x)/\varepsilon_1$ and $(E_{x-y} - E_y)/\varepsilon_2$, respectively. Here, $E_{x\text{-}y}$ is the band gap of hetero bilayers; Ex and Ey are the band gaps of constituents homo bilayers; ε_1 is the induced tensile strain and ε_2 is the induced compression strain. In all the considered hetero bilayers, a negative value of the band gap deformation potential (Table II) indicates the decrease in the band gap value on hetero structuring. The magnitude of the deformation potential is maximum in Type-III bilayers which can be attributed to a small lattice mismatch between the constituent monolayers.

3. Carriers effective mass

It is interesting to note modification in the carrier effective mass on hetero structuring. A knowledge of the carrier effective mass is more exciting and beneficial to account for the conduction process in the realization of devices.

In the present calculations, the effective mass of electron (m_e*) and effective mass of hole (m_h*) were determined from the curvature of the energy band at conduction band minimum (CBM) and valance band maximum (VBM), respectively,[5,34] as follows:

$$m^* = \hbar^2/(\partial^2 E/\partial k^2). \quad (1)$$

Note that our calculated values of the effective masses, in Table III, for homo bilayer structures (Type-I) are consistently lower than the values reported in literature[35] by using hybrid functional. This may be due to the inherent discrepancy in the conventional DFT approach used in our study. It

TABLE II. Calculated % of induced intrinsic strain, electronic band gaps, and DPs of the hetero bilayers.

		Induced strain (%)			DP (eV)	
Bilayer type	Material	ε_1	ε_2	Band gap (eV)	Tensile	Compression
I	MoS_2-MoS_2	…	…	1.49, 1.59[a]	…	…
				1.6[b] (Exp.)		
	$MoSe_2$-$MoSe_2$	…	…	1.25, 1.42[a]	…	…
	WS_2-WS_2	…	…	1.68	…	…
	WSe_2-WSe_2	…	…	1.43	…	…
II	MoS_2-$MoSe_2$	2.17	−2.08	0.60	−0.41	−0.32
		2.24[c]	−2.24[c]	0.63[d]		
	WS_2-WSe_2	2.13	−2.04	0.79	−0.42	−0.31
III	MoS_2-WS_2	0.20	−0.20	1.33	−0.80	−1.74
	$MoSe_2$-WSe_2	0.16	−0.16	1.12	−0.82	−1.54
IV	MoS_2-WSe_2	2.34	−2.23	0.30	−0.51	−0.51
	$MoSe_2$-WS_2	1.96	−1.88	1.06	−0.10	−0.33

[a]Reference 24.
[b]Reference 11.
[c]Reference 20.
[d]Reference 25.

TABLE III. Effective masses of electron (m_e*) and effective mass of holes (m_h*) at CBM and VBM, respectively (all in unit of electron mass m_e) in the hetero bilayers.

Bilayer type	Material	m_e*	m_h*
I	MoS_2-MoS_2	0.23, 0.5155[a]	0.25, 0.547[a]
	$MoSe_2$-$MoSe_2$	0.20, 0.539[a]	0.31, 0.5955[a]
	WS_2-WS_2	0.33, 0.359[a]	0.29, 0.3455[a]
	WSe_2-WSe_2	0.31, 0.4115[a]	0.35, 0.3485[a]
II	MoS_2-$MoSe_2$	0.19	0.15
	WS_2-WSe_2	0.36	0.24
III	MoS_2-WS_2	0.23	0.27
	$MoSe_2$-WSe_2	0.15	0.19
IV	MoS_2-WSe_2	0.27	0.25
	$MoSe_2$-WS_2	0.37	0.33

[a]Reference 33.

is worth mentioning here that our aim is to provide a general insight about the change in the effective mass values on hetero structuring of considered structure which is important for the application of device modelling. It is evident from the Table III that effective mass of hetero bilayers (e.g., Type-II, Type-III, and Type-IV) is generally lower than that of the homo bilayer (Type-I) which may offer large carrier mobilities in electronic devices based on the heterostructures considered.

B. Effect of extrinsic tensile strain on the electronic properties

The strain in 2D structures can be introduced in many ways,[36–44] such as depositing them onto the flexible substrate, by subjecting them to external load, by pseudomorphic growth and nano indentation of the system. The strain engineering has been successfully applied experimentally to graphene.[36–39] The maximum biaxial tensile strain up to 25% in graphene[36] has been observed before breaking of the C-C bond in the sheet. Therefore, in addition to intrinsic strain in hetero structures, it is worth investigating the magnitude of externally applied strain up to which the considered structures do not break.

In the present study, we investigate the strain-stress curves for considered bilayer structures by calculating the response of stress tensor components for applied in-plane biaxial tensile strain. The stress tensor is defined as the positive derivative of total energy with respect to strain tensor.[5,22] In the case of homogeneous biaxial strain, the stress components along two axes are same. The maximum stress that is achieved in response to tensile strain can be calculated from the highest value of stress at which the slope becomes zero in the strain-stress relationship. It is evident from Figure 2 that the ultimate tensile strength of considered structures lies between 9 and 12 GPa, while the strain at which the slope of the strain-stress curve becomes zero is nearly 20% for all types of bilayers considered. The calculated values of ultimate tensile strain (20%) are higher than the effective in-plane strain (6–11%) measured for 2D-MoS_2[40] by using nano-indentation method, however, these values are consistent with the ultimate strain values (20–25%) calculated for theTMDs[5,45] monolayers.

C. Effect of extrinsic strain and electric field on electronic properties

Electronic structure of bilayer TMDs can be effectively altered by various means, such as application of in-plane mechanical strains, by applying vertical compression and electrically gating by perpendicular electric field.[6,24,46–48] The electronic band structure of the bilayer structures was calculated along the Γ-M-K-Γ high symmetry points direction of the Brillouin zone. In the recent studies, tuning of the electronic band structures of homo bilayers (Type-I) by means of the application of in-plane strain, vertical compression, and external electric field was previously reported.[6,24,47] Here, we give a flavour of homo bilayers, especially strain and electric field induced charge density difference profile for an in-depth insight of the physics and chemistry of the bilayers.

1. Band structure

The strain-free/zero-field electronic band structure of homo bilayers (Type-I) shows the VBM and CBM at "Γ" and "K" high symmetry point, respectively, revealing indirect band gap (Figure S1 of supplementary information[49]). The in-plane biaxial tensile strain (+a+b), vertical compression strain (−c), and external electric field considerably reduce the band gap of the homo bilayers, while initial increase in the band gap is predicted for the in-plane biaxial compression strain (−a–b) within the applied strain range, 0–10% (Figure S2 of supplementary information[49]). These results are consistent with the previous reports.[6,15,17,24,47]

Figures 3–5 show the electronic band structure and corresponding partial density of states (PDOS) of hetero bilayers, Type-II, Type-III, and Type-IV, respectively. The electronic band structure and corresponding partial density of states for remaining structures are provided in Figures S3–S5 of the supplementary information[49] which are essentially similar as far as the features are concerned.

All the hetero bilayer structures are found to posses both VBM and CBM at "K" high symmetry point making them to be direct band gap semiconductors. The hetero bilayers (i.e., Type-II, Type-III, and Type-IV) show considerable reduction in the electronic band gap as compared with Type-I homo bilayers. Analysis of the PDOS of hetero structures reveals that the reduction in electronic band gap is probably due to the band offset, i.e., localization of VBM and CBM on different layers.[30] For example, in MoS_2-WSe_2, the contribution to VBM mainly comes from d-states of W and p-states of Se atoms, while for CBM, contribution comes from Mo d-states and p-states of S atoms. Secondly, this may also be attributed to different electro-negativities of chalcogen/metal atoms in two layers which leads to spontaneous electrical polarization at the interface, which generates an induced internal electric field directed from heavier chalcogen/metal atoms to lighter ones.[20]

The band gap of hetero bilayers can be further modulated by the in-plane strain, vertical strain, and external electric field as is apparent from the Figures 3–5, respectively. The direct band gap of all types of hetero bilayers retained up to a very small (2–4%) applied strain (+a+b, −a−b, −c),

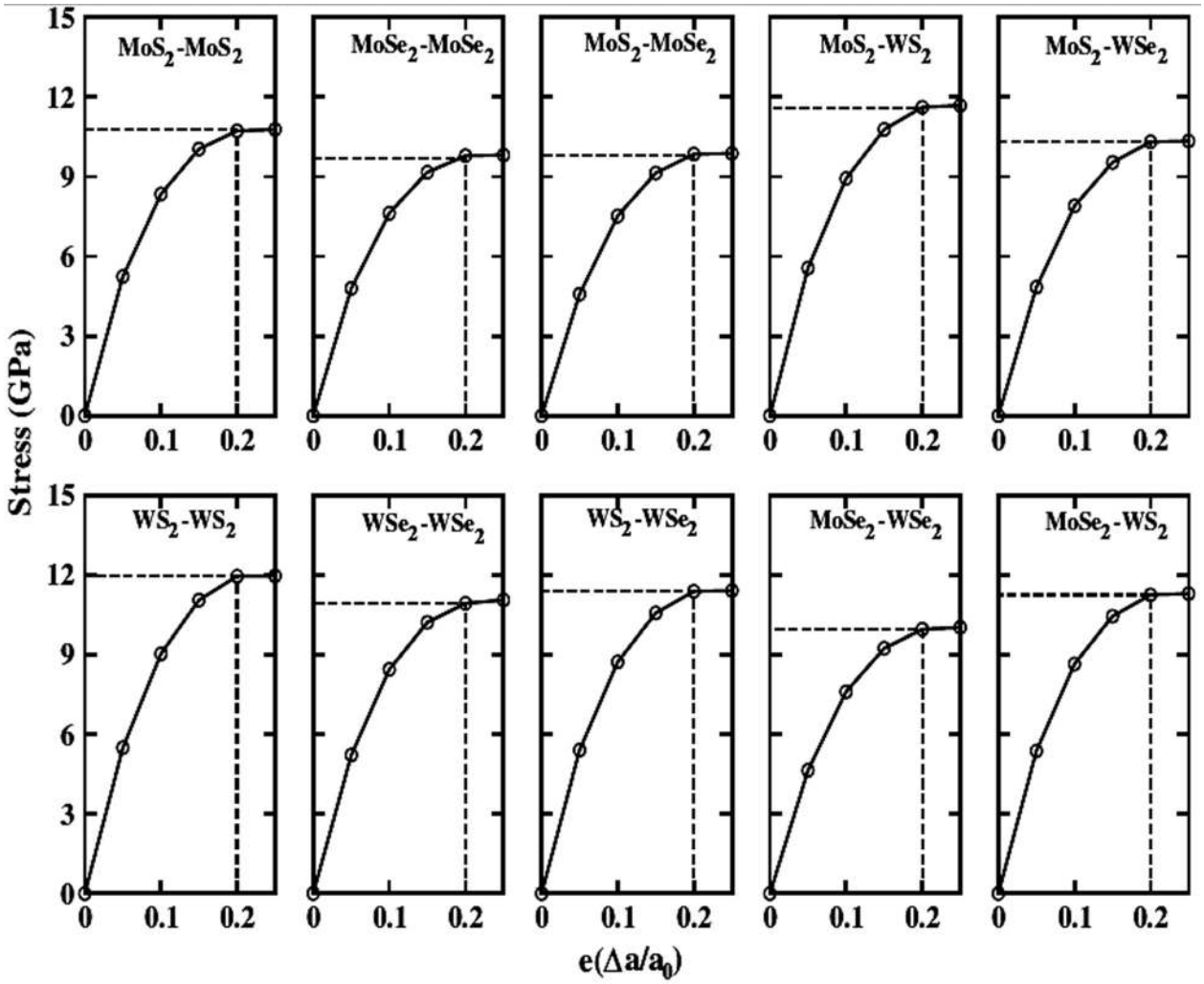

FIG. 2. Strain-stress curve for bi-axial tensile strain (+a+b) applied to four different types of the hetero bilayers.

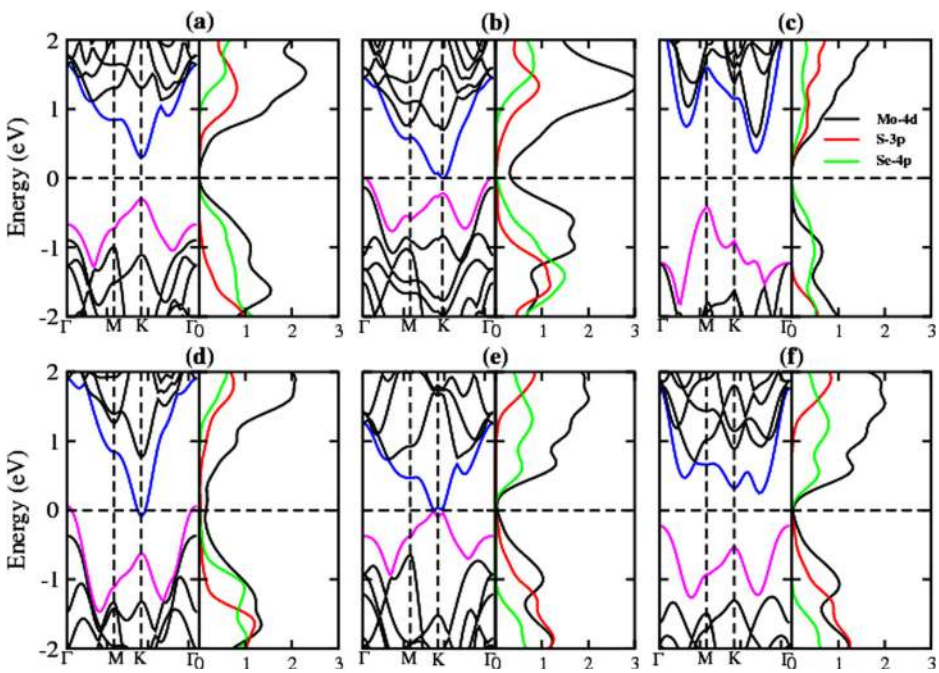

FIG. 3. Electronic band structures and corresponding partial density of states of MoS_2-$MoSe_2$ bilayer (Type-II) at (a) unstrained/zero-field (b) bi-axial tensile (+a+b) strain, (c) biaxial compression (−a−b) strain, (d) vertical compression (−c) strain, (e) positive electric field (+E), and (f) negative electric field (−E) applied to the strain-free hetero bilayers. Band structures shown here are at 10% applied strain and at an electric field of 0.5 V/Å, respectively.

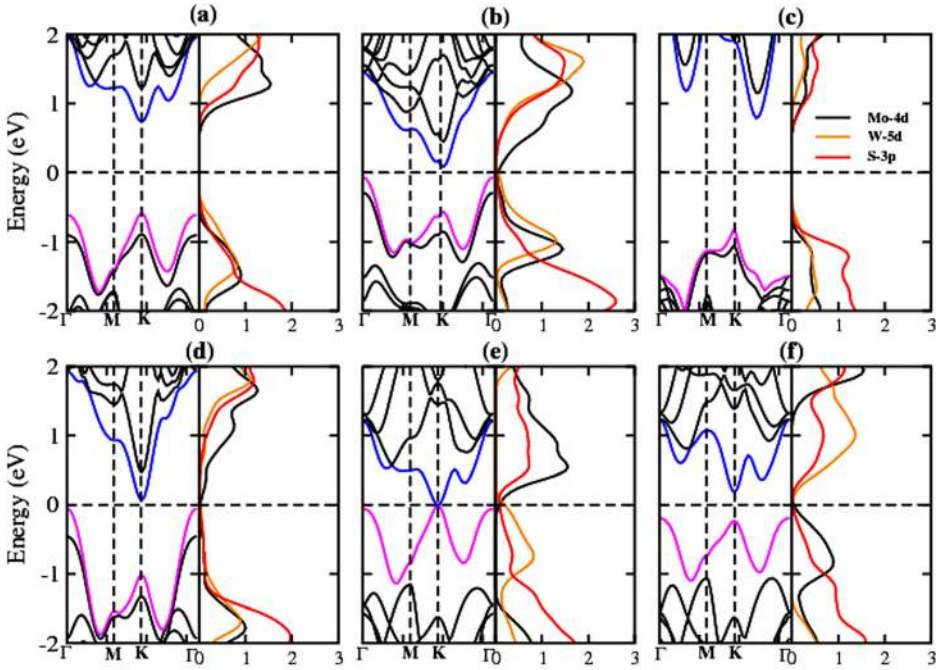

FIG. 4. Electronic band structures and corresponding partial density of states of MoS_2-WS_2 bilayer (Type-III) at (a) strain-free/zero-field (b) bi-axial tensile (+a+b) strain, (c) biaxial compression (−a−b) strain, (d) vertical compression (−c) strain, (e) positive electric field (+E), and (f) negative electric field (−E) applied to strain-free structures. Band structures shown here are at 10% applied strain and at an electric field of 0.5 V/Å, respectively.

while direct-to-indirect band gap transitions occur on further increasing the magnitude of applied strain. The semiconductor-to-metal transition is found to be achieved nearly at 10% of applied in-plane tensile and vertical compression strain. In case of the in-plane compression strain, band gap initially increases for small magnitude of strain before reducing at the higher strain (Figure 6).

Increasing the magnitude of applied positive/negative electric field also results in continuous decrease in band gap followed by the semiconductor-to-metal transition at critical value of the applied field. It is worth reporting that spin-orbit splitting, which is not included in our calculations, on the application external electric field may be important in Mo and W chalcogenides at small field (<0.6 V/Å)[47,48] while it saturates at higher values of applied electric field which might have small influence on the calculated electronic structures in the present context. The change in the magnitude of band gap with positive and negative field is not same as can be seen in Figure 7. The initial increase in band gap except for $MoSe_2$-WS_2 (Type-IV) under the negative field is attributed to the counterbalance of external electric field up to some extent with the internal electric field induced due to the electro-negativity difference of chalcogen/metal atoms in the two layers of hetero bilayers. Interestingly, the band gap decreases monotonically in $MoSe_2$-WS_2 under the negative electric field, which is attributed to the same direction of internal induced electric field due to chalcogen atoms and applied negative electric field.

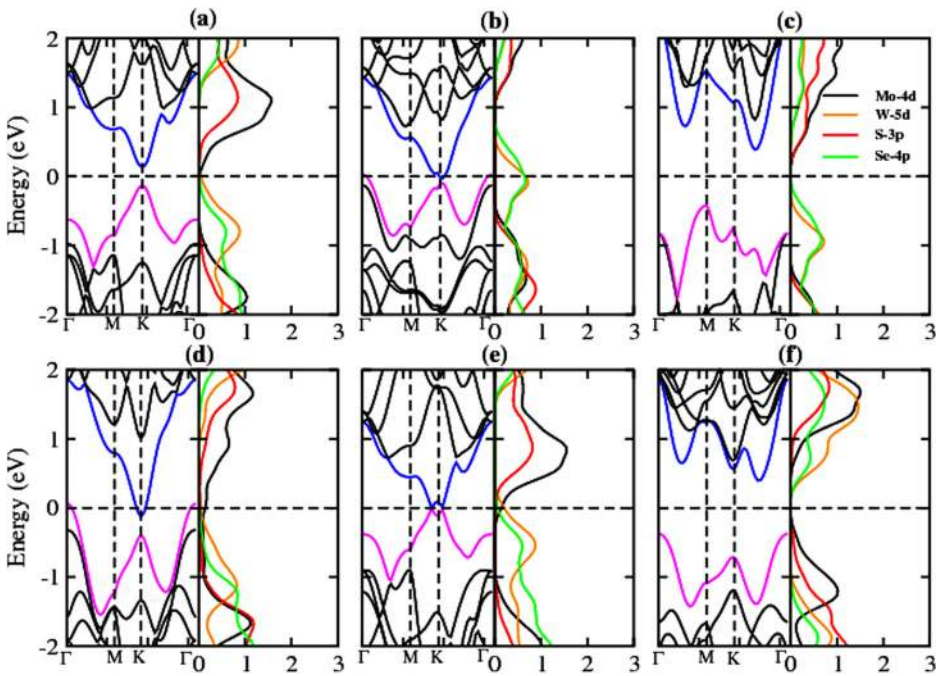

FIG. 5. Electronic band structures and corresponding partial density of states of MoS_2-WSe_2 bilayer (Type-IV) at (a) unstrained/zero-field (b) bi-axial tensile (+a+b) strain, (c) biaxial compression (−a−b) strain, (d) vertical compression (−c) strain, (e) positive electric field (+E), and (f) negative electric field (−E) applied to strain-free structures. Band structures shown here are at 10% applied strain and at an electric field of 0.5 V/Å, respectively.

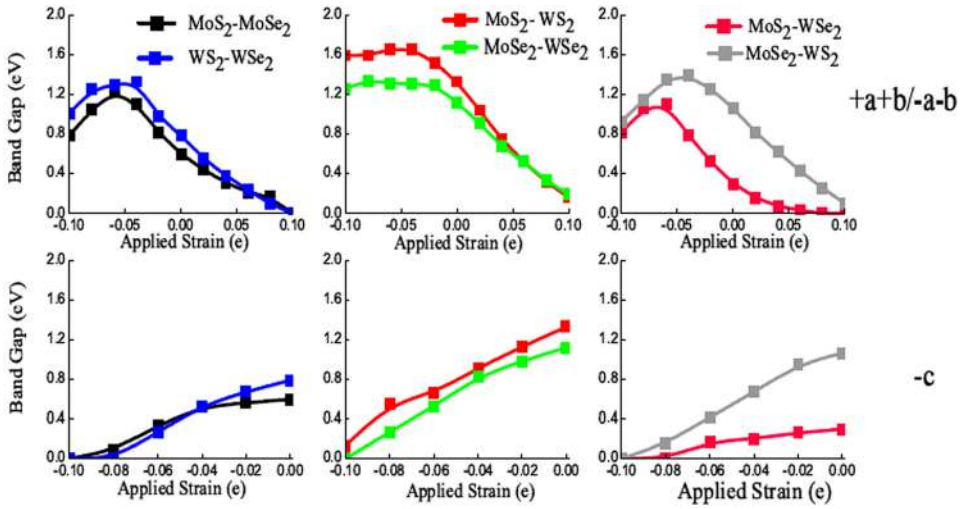

FIG. 6. Plot of electronic band gap versus applied strain for Type-II, Type-III, and Type-IV heterostructures. First row is for bi-axial tensile/compression (+a+b/−a−b) strain. Second row is for vertical compression (−c) strain.

The change in band gap as a function of applied strain and electric field can be understood by analysing the change in PDOS. It has been found that the energy states shift towards (away) from the Fermi level with the applied biaxial tensile (compression) strain and electric field which essentially leads to the change in the band gap of hetero bilayers. These shifts in energy states under applied strain can be attributed to the change in in-plane inter atomic distances which lead to variation in superimposition of their atomic orbitals which explicitly cause shift in energy states.

2. Charge density

The change in band gap by mechanical strain and external electric field can be further understood by examining the charge density difference profile at strain-free/zero-field and mechanically strained as well as electrically gated hetero bilayer structures as shown in Figure 8. The charge density difference is calculated by taking the difference between the total charge density of bilayer structure ($\rho_{MX_2\text{-}M'X'_2}$) and two isolated monolayers (ρ_{MX_2}, $\rho_{M'X'_2}$), i.e., $\Delta\rho = \rho_{MX_2\text{-}M'X'_2} - (\rho_{MX_2} + \rho_{M'X'_2})$. The red and green regions show charge accumulation and charge depletion, respectively.

The increased accumulation of charge between the two layers on the application of tensile strain (+a+b) indicates strong interactions between the layers that change energy bands and hence energy-gap. The increase in band gap on the application of compression strain (−a−b) within considered strain range is reflected by a negligible charge accumulation within the layers. The decrease in energy-gap with vertical compression strain (−c) is attributed to the redistribution of charge on compressing the layers vertically. Also, reduction in band gap was observed on applying both positive electric field (+E) and negative electric field (−E). The band gap reduces in similar magnitude with both the +E and −E field for homo bilayer (Figure S2(c) in supplementary information) which is attributed to homogeneity of the chalcogen/metal atoms on the two surfaces along *z*-direction. The reduction in the band gap is attributed to the redistribution of charge as shown in Figure S3[49] with external electric field. Note that charge redistribution depends on the direction of external electric field. The charge density difference profiles for remaining structures are provided in Figures S6–S9 of the supplementary information[49] which are essentially similar as far as the features are concerned.

3. Deformation potentials

The change in the band structure as a function of extrinsic strain can also be quantified in terms of DP, that has importance in device modeling.[32,33] The change in the energy of a valance band (conduction band) per unit of strain is called valance band deformation potential (conduction band deformation potential).[32] The effect of strain can also be characterized by the change of the transition energy (energy difference) upon application of strain where the linear coefficient provides the deformation potential.[33] For small strain in the vicinity of equilibrium lattice parameters, variation of band gap is approximately linear and hence can be expressed as follows:

$$\Delta Eg = DP \times e, \tag{2}$$

where ΔE_g is change in the band gap, e is the magnitude of strain, and DP is deformation potential. This expression is

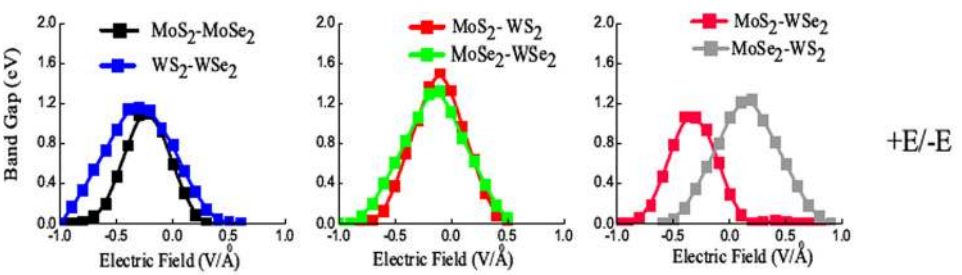

FIG. 7. Plot of electronic band gap versus applied electric field for Type-II, Type-III, and Type-IV heterostructures.

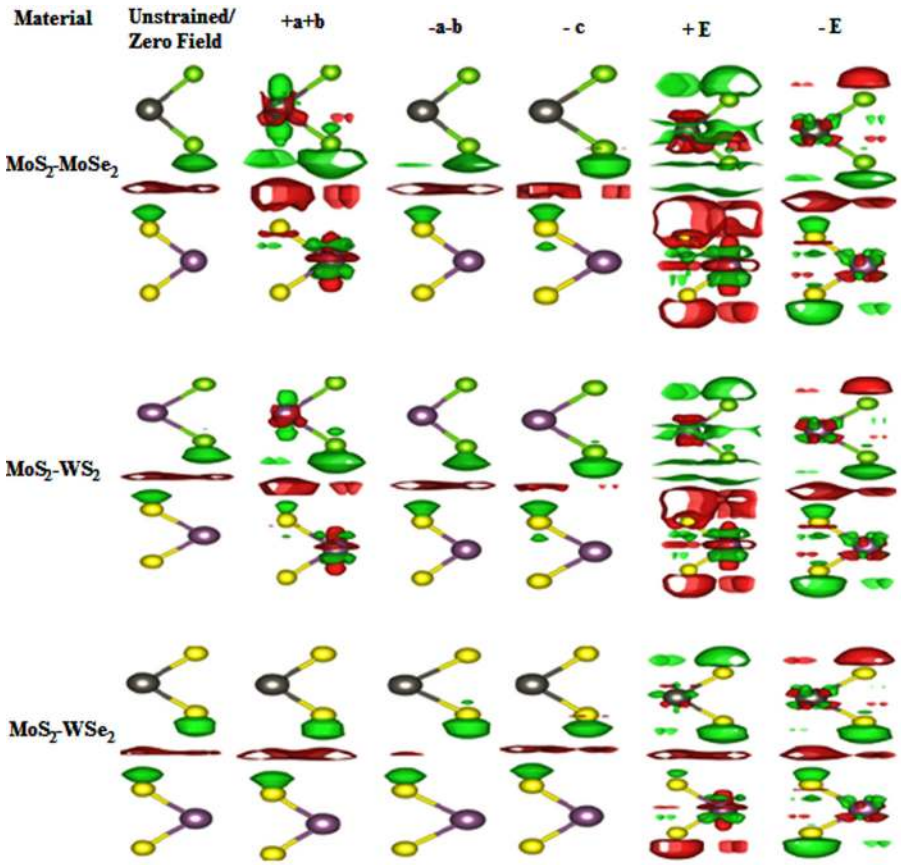

FIG. 8. Charge density difference ($\Delta\rho$) plots for the hetero bilayers with side view. The red (green) distribution corresponds to charge accumulation (depletion). The isosurface is taken as 0.0001 e/ Å^3.

valid for linear regime where the magnitude of strain is typically of the order of 1–2%. The calculated values of DP for both in-plane and vertical strain at 2% value are summarized in Table IV. The positive (negative) values of DP indicate the increase (decrease) in band gap on application of strain.

4. Carrier effective mass

The in-plane strain can also change the curvature of VBM and CBM[5] that can lead to modification in carriers effective masses. We have listed the value of carries effective masses in Table V which are calculated within harmonic limit, i.e., at 2% in-plane tensile and compression strain. Note that the tensile strain reduces effective masses for all the considered bilayers except hole effective masses of homo bilayers. The increase in hole effective masses for homo bilayers under tensile strain is attributed to the change in VBM from "Γ" to "K" high symmetry point due to the application of bi-axial tensile strain. The compression strain increases the carrier effective masses for all the considered structures. It can be concluded that the mechanical strains offer tunability in carrier effective masses and DP's which may lead to tunable mobilities of charge carriers in electronic devices based on the considered hetero structures.

TABLE IV. Calculated band gap DPs in linear regime for biaxial tensile strain, biaxial compression strain, and vertical compression strain applied to the hetero bilayers.

		DP (eV)		
Bilayer type	Material	+a+b	−a−b	−c
I	MoS_2-MoS_2	−15.45	17.30	−10.65
	$MoSe_2$-$MoSe_2$	−14.00	5.75	−11.95
	WS_2-WS_2	−16.65	10.00	−11.45
	WSe_2-WSe_2	−14.40	2.20	−0.25
II	MoS_2-$MoSe_2$	−7.70	10.95	−1.75
	WS_2-WSe_2	−11.8	9.20	−5.65
III	MoS_2-WS_2	−4.50	19.60	−10.25
	$MoSe_2$-WSe_2	−10.35	8.70	−6.85
IV	MoS_2-WSe_2	−7.10	11.35	−2.00
	$MoSe_2$-WS_2	−12.50	9.85	−5.85

TABLE V. Calculated carriers effective masses in linear regime (e = 2%) for bi-axial tensile strain (a+b) and bi-axial compression strain (−a−b) applied to the hetero bilayers. The carrier's effective masses (all in unit of electron mass m_e) have been calculated at VBM and CBM.

		DP (eV)			
		(+a+b)		(−a−b)	
Bilayer type	Material	m_e*	m_h*	m_e*	m_h*
I	MoS_2-MoS_2	0.07	0.28	0.53	0.18
	$MoSe_2$-$MoSe_2$	0.04	0.39	0.25	0.20
	WS_2-WS_2	0.07	0.36	0.53	0.22
	WSe_2-WSe_2	0.07	0.41	0.46	0.24
II	MoS_2-$MoSe_2$	0.05	0.03	0.46	0.30
	WS_2-WSe_2	0.07	0.04	0.63	0.43
III	MoS_2-WS_2	0.04	0.05	0.38	0.47
	$MoSe_2$-WSe_2	0.04	0.05	0.34	0.45
IV	MoS_2-WSe_2	0.05	0.04	0.46	0.42
	$MoSe_2$-WS_2	0.07	0.03	0.62	0.30

IV. SUMMARY

In summary, tuning of the electronic properties of various bilayers of TMDs by intrinsic strain, extrinsic strain, and external electric field are investigated. The band gap reduces considerably as one goes from homo bilayers to hetero bilayers due to the induced intrinsic strain in hetero bilayers. Induced strain is also found to modify carrier effective mass in hetero structures. The band gap of hetero bilayers can further be decreased by applying extrinsic strain and external electric field which leads to semiconductor-to-metal transitions at critical value of applied strain/field. The energy gap in hetero structures remains the same up to nearly 2–4% applied strain. The ultimate tensile strain before breaking the structures is estimated nearly 20% which leads to 9–12 GPa tensile strength of the hetero structures considered. Extrinsic strain also modifies the carrier effective masses of the hybrid bilayer structures.

ACKNOWLEDGMENTS

We are grateful to SIESTA team for providing code. Munish Sharma also acknowledges financial support from DST New Delhi in the form of INSPIRE Fellowship.

[1]*MoS_2: Material, Physics and Devices*, edited by Z. M. Wang (Springer, 2014), Vol. 21.
[2]A. Kumar and P. K. Ahluwalia, Eur. Phys. J. B **85**, 186 (2012).
[3]A. Kumar and P. K. Ahluwalia, Physica B **407**, 4627 (2012).
[4]A. Kumar and P. K. Ahluwalia, Mater. Chem. Phys. **135**, 755 (2012).
[5]A. Kumar and P. K. Ahluwalia, Physica B **419**, 66 (2013).
[6]A. Kumar and P. K. Ahluwalia, Model. Simul. Mater. Sci. Eng. **21**, 065015 (2013).
[7]A. Kumar and P. K. Ahluwalia, J. Alloys Compd. **550**, 283 (2013).
[8]A. Kumar and P. K. Ahluwalia, J. Alloys Compd. **587**, 459 (2014).
[9]D. Jariwala, V. K. Sangwan, L. J. Lauhon, T. J. Marks, and M. C. Hersam, ACS Nano **8**(2), 1102 (2014).
[10]K. S. Novoselov, D. Jiang, F. Schedin, T. J. Booth, V. V. Khotkevich, S. V. Morozov, and A. K. Geim, Proc. Natl. Acad. Sci. U.S.A. **102**(30), 10451 (2005).
[11]K. F. Mak and C. Lee, Phys. Rev. Lett. **105**, 136805 (2010).
[12]J. Wilson and A. D. Yofee, Adv. Phys. **18**(73), 193 (1969).
[13]S. Bertolazzi, D. Krasnozhon, and A. Kis, ACS Nano **7**, 3246 (2013).
[14]T. Georgiou, R. Jalil, B. D. Belle, L. Britnell, R. V. Gorbachev, S. V. Morozov, Y. J. Kim, A. Gholinia, S. J. Haigh, O. Makarovsky, L. Eaves, L. A. Ponomarenko, A. K. Geim, K. S. Novoselov, and A. Mishchenko, Nat. Nanotechnol. **8**, 100 (2013).
[15]E. Scalise, M. Houssa, G. Pourtois, V. Afanasev, and A. Stesmans, Nano. Res. **5**(1), 43 (2012).
[16]P. Johari and V. B. Shenoy, ACS Nano **6**(6), 5449 (2012).
[17]P. Lu, X. Wu, W. Guo, and X. C. Zeng, Phys. Chem. Chem. Phys. **14**, 13035 (2012).
[18]H. Terrones, F. L. Urias, and M. Terrones, Sci. Rep. **3**, 01549 (2013).
[19]H. P. Komsa and A. V. Krasheninnikov, Phys. Rev. B **88**, 085318 (2013).
[20]L. Kou, T. Frauenheim, and C. Chen, J. Phys. Chem. Lett. **4**, 1730 (2013).
[21]A. A. Jeffery, C. Nethravathi, and M. Rajamathi, J. Phys. Chem. C **118**, 1386–1396 (2013).
[22]J. M. Soler, E. Artacho, J. D. Gale, A. Garclia, J. Junquera, P. Ordejon, and D. S. Portal, J. Phys.: Condens. Matter **14**, 2745 (2002).
[23]N. Troullier and J. L. Martins, Phys. Rev. B **43**, 8861 (1991).
[24]S. Bhattacharya and A. K. Singh, Phys. Rev. B **86**, 075454 (2012).
[25]C. Lee, J. Hong, M. H. Whangbo, and J. H. Shim, Chem. Mater. **25**, 3745 (2013).
[26]Y. H. Zhao, F. Yang, J. Wang, H. Guo, and W. Ji, e-print arXiv:1310.7285v1 (2013).
[27]R. G. Amorim, X. Zhong, S. Mukhopadhyay, R. Pandey, A. R. Rocha, and S. P. Karna, J. Phys.: Condens. Matter **25**, 195801 (2013).
[28]D. Xu, H. He, R. Pandey, and S. P. Karna, J. Phys.: Condens. Matter **25**, 345302 (2013).
[29]B. Mohan, A. Kumar, and P. K. Ahluwalia, Physica E **44**, 1670 (2012).
[30]K. Kosmider and J. Fernandez-Rossier, Phys. Rev. B **87**, 075451 (2013).
[31]H. Peelaers and C. G. Van de Walle, Phys. Rev. B **86**, 241401(R) (2012).
[32]M. V. Fischetti and S. E. Laux, J. Appl. Phys. **80**, 2234 (1996).
[33]Q. Yan, P. Rinke, M. Scheffer, and C. G. Van de Walle, Appl. Phys. Lett. **95**, 121111 (2009).
[34]A. Ramasubramaniam, Phys. Rev. B **86**, 115409(R) (2012).
[35]D. Wickramaratne, F. Zahid, and R. K. Lake, e-print arXiv:1401.0502v1 (2014).
[36]C. Lee, X. Wei, J. W. Kysar, and J. Hone, Science **321**, 385 (2008).
[37]T. M. G. Mohiuddin, A. Lombardo, R. R. Nair, A. Bonetti, G. Savini, R. Jalil, N. Bonini, D. M. Basko, C. Galiots, N. Marzari, K. S. Noveselov, A. K. Geim, and A. C. Ferrari, Phys. Rev. B **79**, 205433 (2009).
[38]G. Tsoukleri, J. Parthenios, K. Papagelis, R. Jalil, A. C. Ferrari, A. K. Geim, K. S. Novoselov, and C. Galiotis, Small **5**, 2397 (2009).
[39]M. Huang, H. Yan, T. F. Heinz, and J. Hone, Nano Lett. **10**, 4074 (2010).
[40]S. Bertolazzi, J. Brivio, and A. Kis, ACS Nano **5**, 9703 (2011).
[41]J. Fang, X. Qian, C. W. Huang, and J. Li, Nat. Photonics **6**, 866 (2012).
[42]K. K. Liu, W. Zhang, Y. H. Lee, Y. C. Lin, M. T. Chang, C. W. Su, C. S. Chang, H. Li, Y. Shi, H. Zhang, C. S. Lai, and L. J. Li, Nano Lett. **12**, 1538 (2012).
[43]Y. H. Lee, X. Q. Zhang, W. Zhang, M. T. Chang, C. T. Lin, K. D. Chang, Y. C. Yu, J. T. W. Wang, C. S. Chang, L. J. Li, and T. W. Lin, Adv. Mater. **24**, 2320 (2012).
[44]Y. Zhan, Z. Liu, S. Najmaei, P. M. Ajayan, and J. Lou, Small **8**, 966 (2012).
[45]J. Li, N. V. Medhekar, and V. B. Shenoy, J. Phys. Chem. C **117**, 15842 (2013).
[46]Q. Liu, L. Li, Y. Li, Z. Gao, Z. Chen, and J. Lu, J. Phys. Chem. C **116**, 21556 (2012).
[47]A. Ramasubramaniam, D. Naveh, and E. Towe, Phys. Rev. B **84**, 205325 (2011).
[48]N. Zibouche, P. Philipsen, A. Kuc, and T. Heine, e-print arXiv:1406.5012v1 (2014).
[49]See supplementary material at http://dx.doi.org/10.1063/1.4892798 for Electronic band structures, PDOS band gap, and charge density difference profiles of various-bilayer systems (Figures S1–S9).